Fuel 373 (2024) 132356

Contents lists available at ScienceDirect

Fuel

journal homepage: www.elsevier.com/locate/fuel

Full Length Article

Assessing the recyclability of spent fluid catalytic cracking catalyst for sustainable dry reforming of methane

Ahmed Abotaleb [a], Nada Abounahia [a], Sjood Makeen [b], Janarthanan Ponraj [c], Mabkhout Al Yarabah [a], Francesco Ferella [d], Alessandro Sinopoli [a,*]

[a] Qatar Environment and Energy Research Institute, Hamad Bin Khalifa University, P.O. Box 34110, Doha, Qatar
[b] Department of Chemistry and Earth Sciences, College of Arts and Sciences, Qatar University, Doha, P.O. Box 2713, Qatar
[c] HBKU Core Labs, Hamad Bin Khalifa University, P.O. Box 34110, Doha, Qatar
[d] Department of Industrial and Computer Engineering and Economics, University of L'Aquila, P.le E. Pontieri 1, Monteluco di Roio, 67100 L'Aquila, Italy

ARTICLE INFO

Keywords:
Dry reforming of methane
Zeolite
Recycled catalyst
Sustainability
Fluid catalytic cracking catalysts

ABSTRACT

Spent catalysts are a significant source of metal-containing waste, and their disposal can pose environmental and economic challenges. Recycling these spent catalysts can not only reduce waste but also recover valuable metals, which can be used as raw materials for synthesizing new catalysts, as well as produce substrates for other industrial catalytic applications. Here we explore the recycling of spent fluid catalytic cracking catalysts (FCCCs) to obtain zeolite-based materials. Such substrates have been further doped with nickel via wet impregnation method to generate fresh catalysts for dry reforming of methane (DRM) reaction. Comprehensive analyses, including X-ray diffraction (XRD), BET surface area, scanning and transmission electron microscopy (SEM and TEM), H_2-temperature programmed reduction (H_2-TPR), NH_3-temperature programmed desorption (NH_3-TPD), and Ni dispersion via H_2-pulse chemisorption, were employed to characterize these catalysts. The performance of these recycled zeolite materials was evaluated and benchmarked against commercial zeolites. Our findings reveal that acid-leached, recycled zeolite obtained from spent FCCC catalyst results in the highest overall CO_2 and CH_4 conversion among the studied catalysts, as well as exhibiting a high stability over 20-hour testing, underscoring the potential of recycling strategies in catalyst production.

1. Introduction

Sustainability is a holistic approach to meeting the current global needs without jeopardizing the capacity of next generations to satisfy their own needs. This involves responsible resource managment, environmental guardianship, and the promotion of social fairness. Embracing sustainability aims to create a balanced and harmonious coexistence between human activities and the natural world [1]. The guidelines for sustainability have been indicated in the 2030 Agenda for Sustainable Development, adopted by all United Nations Member States in 2015 to achieve the seventeen goals described in the final document [2]. Technology is crucial in helping us to develop greener, less energy-intensive processes for many of the agreed goals.

Circular economy is another concept developed in recent years and derived from the awareness of our planet's limited or scarce natural resources. Based on that, the linear economy, i.e., production, use, and disposal of, is not viable anymore, instead a circular approach is now required, i.e., based on a loop that links the production of goods to their final recycling and reuse.

The strict circular approach foresees the recycling and reuse of materials to produce the same original product. Nevertheless, this is not always possible, as sometimes the current technologies cannot restore the identical original properties needed for a working and affordable item. For instance, manganese recovered from spent alkaline batteries could not be electrolytically active to manufacture new batteries, but such recycled MnO_2 could be used as a pigment in paint and ceramic industries or as a feedstock for other manganese compounds [3]. Hence, the meaning of circular economy is now broader and is focused on recycling as many recovered materials as possible in the manufacturing processes, limiting the fraction incinerated or disposed of directly. Nowadays, each productive sector is looking for technological solutions to reduce its environmental footprint, including the refining ones, which is among the most polluting.

Over the past few decades, the expansion of the industrial,

* Corresponding author.
E-mail address: asinopoli@hbku.edu.qa (A. Sinopoli).

https://doi.org/10.1016/j.fuel.2024.132356
Received 9 March 2024; Received in revised form 23 May 2024; Accepted 25 June 2024
Available online 2 July 2024

commercial, and agricultural fields has led to an increased production of petrochemicals, refined fuels (including gasoline, diesel, kerosene, jet fuel, and naphtha), and intermediary materials. This growth has spiked the need for catalysts in refining processes. Although some catalysts can undergo regeneration through specific thermal processes using nitrogen, air, or oxygen, repeated regenerations may ultimately diminish their catalytic effectiveness irreversibly. Other types of catalysts, like those used in fluid catalytic cracking (FCC), are prone to contamination by heavy metals like nickel and vanadium, rendering them unable to be regenerated and necessitating periodic replacement with fresh catalysts [4]. The incorporation of rare earth oxides (REO) in FCC catalysts was motivated by the pursuit of more efficient and thermally stable products that exhibit improved yield performance. The concentration of REOs has progressively increased over the years and currently averages between 3–5 % by weight [5].

FCCCs are typically based on zeolites, especially type X, type Y and ZSM-5, these are characterized by different silica–alumina ratios and different ions on their surface. Some recycling routes were proposed in the past for spent FCCCs, such as partial replacement of cement in mortars, as new catalysts for other catalytic processes after regeneration or treatments, for zeolite production or the sole extraction of cerium and lanthanum [6]. Nevertheless, the current market prices can not justify the exclusive extraction of La and Ce from spent FCCC, given their relatively low concentration. As a result, such catalysts accumulate in huge heaps next to the petrochemical plants and are thus disposed of occasionally. For example, Bapco's plant in Bahrain, refining 267,000 barrels of crude oil per day, produces around 100 tonnes/month of exhaust FCCC [7]. In Europe, this kind of catalyst is collected by authorized companies whose services, e.g., collection from petrochemical plants, safe transportation, and final disposal into landfills for hazardous waste, now cost 300 to 450 Euro/tonne. FCC catalysts are among the few not currently recycled because of their low intrinsic value. Nevertheless, Rare Earth Elements (REEs) have been included in the recently updated list of 27 critical raw materials disclosed by the European Commission [8]. This underscores the imperative for their recycling in the near future by every country that wants to face the technological challenge of the green industrial revolution.

The group of Ferella has reported the recovery of cerium and lanthanum from spent FCCCs by leaching with sulfuric acid, where around 80 % of the REEs were recovered [9,10]. Nevertheless, the environmental problem is not solved yet, despite the recovery of REEs, as more than 95 % of the material's mass is still there as a solid residue after the leaching stage. It is possible to take advantage of such a residue to produce synthetic zeolites. These are crystalline microporous aluminosilicates consisting of tetrahedral SiO_4 and AlO_4 with an oxygen atom acting as an interconnecting bridge between the tetrahedra [11], widely used in many industrial processes like water treatments, several catalysis and gas adsorption [12]. One of the first research group that proposes such a technique was the group of Basaldella in 2006 [13]. With this technique, the produced zeolites were mainly characterized by Na-A or as Na-X crystalline phases [5]. An accurate study demonstrated the economic profitability of such an entire recycling process that recovers La and Ce as a mixed oxide and produces synthetic zeolites [12]. It is worthy of note that spent catalysts are a significant source of metal-containing waste, and their disposal can pose environmental and economic challenges. By recycling these materials, not only is waste minimized, but valuable metals are reclaimed. These recovered metals can serve as essential raw materials in the manufacture of new catalysts or for various industrial uses.

Owing to their distinctive physical and chemical attributes, zeolites have garnered extensive interest and application as catalysts in a range of industrial operations, notably in the process of methane reforming. [14] In this regard, dry reforming of methane (DRM) has been a focal point of research for numerous years, driven by the rising global need for hydrogen, environmental conservation, and the conversion of abundant global natural gas reserves into fuels and other hydrocarbons [15]. DRM is a valuable process to produce industrial demanded syngas, an important mixture of CO and H_2 (ratio of unity). However, DRM requires a conspicuous amount of energy, with reaction temperatures ranging from 550 to 900 ℃, resulting in high coke formation and catalyst deactivation [16].

$$CO_2 + CH_4 \rightarrow 2CO + 2H_2.$$

Noble metals (such Ru, Rh, Pd and Pt) and Ni-based catalysts are frequently used as DRM catalysts. However, the widespread use of noble metals has been constrained by their expensive pricing and sinterization issues [17]. Ni-based catalysts are distinguished by their abundancy, low price, and high activity; however, carbon deposition and Ni sintering are still major concerns for their utilization in DRM at high temperatures. Therefore, considerable research attention for employing more effective supports with high surface area and thermal conductivity has recently taken place. These supports materials are also designed in order to minimize the coke formation and sintering, to increase catalyst lifetime. For usage in DRM, nickel catalysts with several support materials, such as MgO, TiO_2, Al_2O_3, SiO_2, MOFs, and various types of zeolites were studied [11,18–22].

Zeolites have been found to be an effective support catalysts for methane reforming due to their well define pore structure, plentiful supply, chemical/thermal stability, and high surface area (approx. 460–800 m^2/g), and acidity [11,19,32]. The acidic sites on the zeolite surface can promote the adsorption and activation of methane molecules, while the microporous structure of zeolites can provide confinement and selectivity to the reaction intermediates, leading to higher activity and selectivity in the methane reforming process [11]. The incorporation of Ni metal on zeolite supports can provide several advantages such as improved thermal stability, better metal dispersion, and enhanced reaction selectivity [23].

Zeolites can also regulate the formation and distribution of reactive intermediates and control the coke deposition on the catalyst surface [11]. In addition, previous findings indicated that the specific choice of zeolite materials as catalyst support might impact both the hydrophobicity of the resulting catalyst as well as on the location and reducibility of Ni nanoparticles [33–35]. Indeed, zeolite-supported nickel (Ni) catalysts are emerging as highly effective in methane reforming, thanks to their robust catalytic properties. Particularly, ZSM-5 zeolites are beneficial as support for Ni-based catalysts because their high silicon to aluminium (Si/Al) ratios, which contribute to the essential acidity and spatial confinement needed for the reactions. Research has not only been confined to ZSM-5 but has also extended to other zeolite structures like beta, Y, and SAPO-34, exploring their capability to enhance methane reforming. [11,16]. Pinheiro *et al.* [24]and Frontera *et al.* [25]emphasized the use of these zeolite supports for the production of hydrogen by dry reforming of methane, indicating the versatility of zeolites in catalytic applications. In a novel approach, Wei *et al.* [26] developed a silicon carbide (SiC) coating on zeolites using hydrothermal synthesis, which, in a 30-hour dry reforming of methane (DRM) test, revealed that their honeycomb-like Ni/S-1/SiC catalysts exhibited superior activity and longevity. Meanwhile, Kweon *et al.* [27] introduced a method for synthesizing Ni-containing beta zeolite (Ni-BEA) through a single-step interzeolite transformation of nickel silicate, using it as a catalyst for dry methane reforming and finding it effective at stabilizing metallic Ni clusters via defect hydroxyls. Additionally, Najfach *et al.* [28] have been examining the role of manganese in zeolite-supported Ni catalysts for dry reforming of methane, pointing out how zeolite composition plays a crucial role in catalytic efficiency.

Further research is still needed to optimize the catalyst design and improve the efficiency and selectivity of the process. Therefore, many studies showed the introduction of a promoter along with nickel on zeolites supports. Liang, Wang *et al.* and Liu *et al.* [29,30] have shown how cobalt addition to different nickel-zeolite catalysts led to improved stability against deactivation with maintaining higher activity over

extended run times. Other promoters used were manganese [28], and ceria-zirconia [31], which enhance properties like metal-support interactions, basicity and nickel dispersion on zeolites supports. However, to the best of our knowledge modifying the recycled synthetic zeolites from spent FCCC as catalyst support for DRM has been rarely reported. Fluid catalyst cracking is one of the main refinery processes that uses massive catalysts and hence produces large amounts of spent catalysts as metal-containing wastes that need to be disposed of. Therefore, recovering spent FCCC could be a beneficial source for obtaining zeolite-based materials to produce new catalysts [5]. The following sections are showing the possibility of reusing the solid residue from spent FCCCs as zeolites supports for Ni-based catalysts by comparing their structural and textural properties to the commercial zeolites as well as their activity performance in DRM.

In this study, we conduct a detailed comparison of the catalytic efficiency of recycled zeolite-based materials from spent FCCCs, both before and after sulfuric acid treatment, with commercial zeolite catalysts, specifically Beta Zeolite and ZSM-5. We impregnated four zeolite samples with nickel salt. The produced catalysts, named Ni-ZSM5, Ni-BetaZ, Ni-RFCC, and Ni-ARFCC, underwent thorough characterization and were tested for dry reforming of methane. Techniques such as XRD, BET analysis, SEM, TEM, H_2-TPR, NH_3-TPD, and TGA were used to examine their properties and the impact of different zeolite supports. The findings highlight how treatment types significantly influence the catalysts' activity and stability, impacted by factors like Ni dispersion, reducibility, and the presence of active sites. Most importantly, this research demonstrates the potential of utilizing recycled zeolites from spent FCCCs as effective substrates for DRM catalysts.

2. Methodology

2.1. Materials and methods

Urea and Nickel(II) chloride hexahydrate 98 % were purchased from Thermo Fischer Scientific and Sigma Aldrich, respectively. The two commercial zeolites materials: Zeolite beta (SiO_2/Al_2O_3 = 25, surface area 580 m^2 /g) and Zeolite Socony Mobil–5 (ZSM-5) (SiO_2/Al_2O_3 = 30, surface area 412 m^2 /g), were supplied by Alfa Aesar and were used in the powder-ammonium form, while the recycled zeolites are referred as RFCC, namely a spent fluid catalytic cracking catalyst (FCCC) from a refinery located in the Persian Gulf and ARFCC: the latter is a synthetic zeolite produced from the same spent FCCC via hydrothermal synthesis. The spent FCCC sample was leached with 1.5 mol/L of H_2SO_4 with a solid to liquid (S/L) ratio equal to 200 g/L, under constant stirring for 3 h at 80 °C. After filtration, the leach liquor underwent recovery of cerium and lanthanum. The solid residue, instead, underwent thermal treatment, which was carried out at 750 °C for 1.5 h with powdered sodium hydroxide, followed by the hydrothermal activation at 95 °C for 12 h. After cooling, the solid was manually crushed and accurately washed with distilled water in order to remove caustic solution, until the water reached a pH value around 7. After drying, the sample was ready for nickel deposition. The detailed synthesis procedure is reported in Ferella *et al.* [5].

2.2. Catalyst preparation

The Ni-ZSM-5 and Ni-BetaZ were prepared by wet impregnation method using Nickel(II) chloride hexahydrate as the metal precursor as shown in Fig. 1. Specifically, 1 g of the commercial zeolites (Beta-zeolite /ZSM-5) were dispersed in 100 mL deionized (DI) water and kept for stirring at room temperature for 20 min at 600 rpm. The nickel salt (nominal 15 wt%) solution was added dropwise to the zeolites aqueous solution and left for stirring for additional 20 min. Impregnation was followed by chemical reduction step to yield Ni metallic nanoparticles on the zeolite materials surface using urea. Urea was added dropwise to the nickel salt mixture in a 1:2.5 wt ratio over about 30 min, followed by an hour of stirring. The mixture was then heated under reflux for 10 h. Subsequently, the solid product was filtered, thoroughly rinsed until the pH neared 7, and the impregnated samples were dried at 105 °C for 12 h before calcination at 800 °C for 6 h. This method was also used for preparing recycled zeolite-supported Ni-based catalysts, and the samples were denoted as Ni-RFCC for the commercial reused FCC sample,

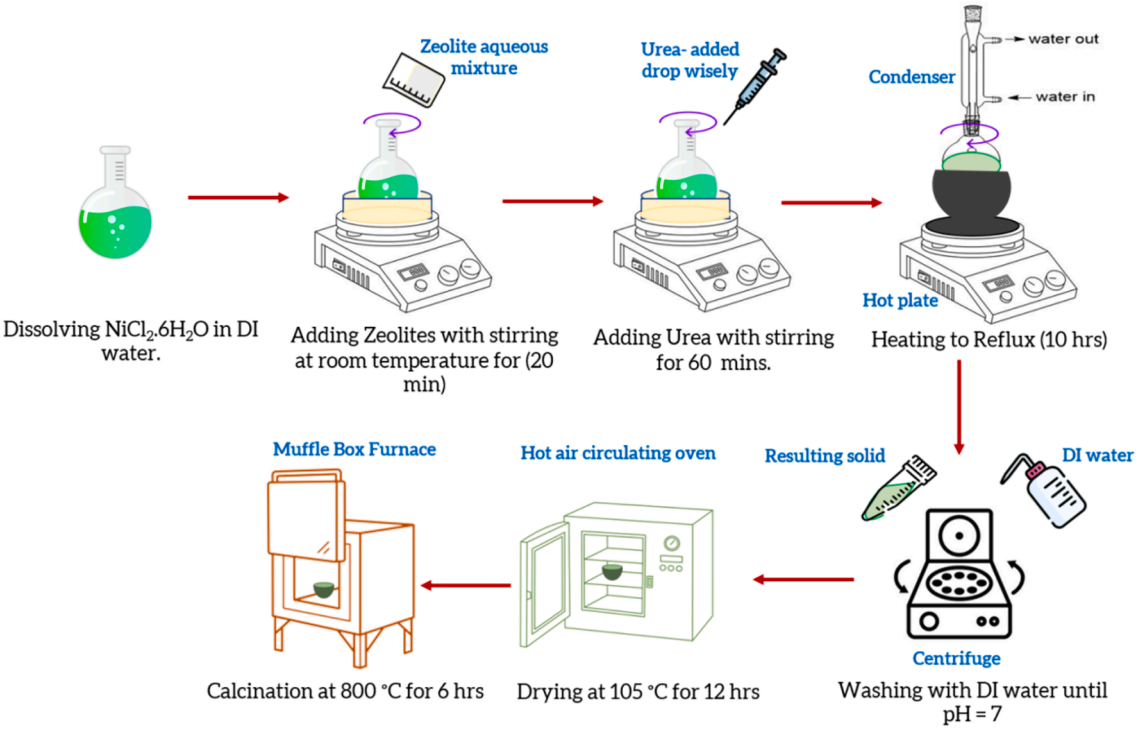

Fig. 1. Schematic diagram of the preparation process for Ni@Zeolites catalysts by impregnation method.

usually based on zeolite-Y, and Ni-ARFCC for the H_2SO_4-treated synthetic zeolite sample.

2.3. Catalysts characterization

For X-ray diffraction (XRD) analysis, a Shimadzu XRD-6100x diffractor was employed, utilizing Cu-Kα (λ = 1.5406 Å) radiation, and set to operate at 40 kV and 30 mA with a scanning speed of 7°/min, covering a range from 3° to 90°.

Transmission electron microscopy (TEM) images were captured with a JEOL 2010 microscope, operating at 200 kV. The sample preparation for TEM involved dispersing the catalysts in ethanol, depositing droplets on a copper grid, and allowing the ethanol to evaporate before inserting the grid into the microscope. Moreover, scanning electron microscopy, as well as actual Ni content on both as-prepared and spent catalysts, was performed by SEM-EDS FEI Quanta650FEG for imaging and equipped with a Bruker XFlash 6I60 detector for EDS analysis.

Thermogravimetric analysis (TGA) of both fresh and spent catalysts was performed using a Discovery TGA from TA Instruments. The catalysts (~10 mg) were heated up to 900 °C at a rate of 10 °C/min with air flow (20 mL min^{-1}).

The X-ray photoelectron spectroscopy (XPS) measurement was performed on a standard Thermo Fisher ESCALAB 250XI type XSP platform. A monochromatic Al Kα anode X-ray beam is used with a beam energy of 1486.6 eV and an energy resolution better than 0.5 eV. The XPS spectra are acquired with a 180° hemispherical electron energy analyser with a normal emission angle and a beam incident angle of 45° to the surface normal. High-resolution C1s, O1s, Si2p, Al2p, Ni2p core level spectra are taken with a pass energy of 20 eV and a step size of 0.1 eV. The energy positions are calibrated with respect to the C1s at 284.8 eV. All the measurements were conducted at room temperature in a UHV chamber of 10^{-10} mbar.

Micromeritics ASAP 2420 analyser was used to determine the specific BET surface areas of the catalysts, which involved a pre-treatment process of drying at 90 °C for 30 min and then degassing at 250 °C for 6 h under vacuum to eliminate contaminants and moisture. The specific surface area calculations were based on the BET equation, while pore size distribution was analysed using BJH desorption. Measurements were performed at 77 K.

H_2 temperature-programmed reduction (H_2-TPR) experiments were carried out using an AutoChem 2950 apparatus, equipped with a thermal conductivity detector. The procedure involved pre-treating 50 mg of catalyst in N_2 (100 mL/min) at 300 °C for 60 min to remove impurities. After cooling, catalyst was reduced in a 10 vol% H_2-Ar mixture (100 mL/min), heating up to 800 °C at a rate of 10 °C/min.

NH_3 temperature-programmed desorption (NH_3-TPD) was conducted to identify the acid sites on the catalysts, using the same AutoChem 2950 apparatus. This involved pre-treating 500 mg of catalyst in N_2 (100 mL/min) at 300 °C for 30 min, then saturating with NH_3/He 10/90 vol% (100 mL/min) at room temperature for 30 min, followed by a flush with He to remove excess NH_3. The samples were then heated up to 800 °C in He, 10 °C/min ramp, with the NH_3 desorption monitored via the thermal conductivity detector.

Pulse chemisorption analysis was carried out using a Micromeritics AutoChemII 2950 station. In this procedure, the catalysts were positioned in a U-shaped stainless-steel reactor to evaluate their Ni dispersion. Initially, 50 mg of catalyst underwent reduction in a 10 vol% H_2-Ar flow at 50 mL/min, heating to 750 °C at 10 °C/min, then purged with Ar to eliminate residual H_2 at 775 °C for an hour before being cooled to room temperature. The chemisorption process took place at 35 °C, utilizing a Micromeritics cryo-cooler to inject liquid nitrogen for temperature control. The setup used a 0.5 cm^3 injection loop and argon as the carrier gas for H_2 pulses (10 vol% H_2 in Ar). The consumption of H_2 during the process was monitored via a thermal conductivity detector (TCD) with a water trap, with all parameters, including sample temperature, pulse injections, and TCD readings, being regulated and recorded through Micromeritics AutoChem software.

2.4. Catalytic evaluation

Evaluations of catalytic activity for the dry reforming of methane (DRM) using Ni-zeolite catalysts were performed in a fixed-bed reactor, sized with an internal diameter of 6 mm and a length of 300 mm. In each test, 200 mg of the catalyst was placed in the MicroEffi reactor and underwent in-situ reduction with 5 % H_2/Ar at a flow rate of 100 mL/min at 800 °C, followed by cooling to 750 °C using argon. An equimolar CH_4/CO_2 gas mixture was then introduced at 50 mL/min. The catalytic efficiency was assessed at 750 °C, over 20 h and gas hourly space velocity (GHSV) of 30,000 mL/h·g_{cat}, analysing the output gases—CO, H_2, CH_4, and CO_2—via an online mass spectrometer. The analysis included determining the conversions of CH_4 and CO_2, space–time yields for H_2 and CO, and the H_2/CO molar ratio, based on inlet and outlet flow rates [36].

3. Result and discussion

3.1. Structural analysis

Catalysts' XRD patterns are illustrated in Fig. 2. As seen in Fig. 2 (A), both ZSM-5 and Beta zeolite supports show typical aluminosilicate peaks between 7 and 30° [28]. While the main crystalline phase found in the RFCC sample well matches with the standard zeolite-Y phases(5-35°) [28,37]. Sample ARFCC revealed the typical pattern of zeolite Na-A. This is caused by the chemical treatment yielding ARFCC, where RFCC is first treated with sulphuric acid and the resulting solid calcinated with NaOH. After doping the substrates with nickel, Fig. 2 (B), Ni-ZSM and Ni-BetaZ samples generally retain the pattern of the pristine samples, with the addition of three minor peaks at 37, 43 and 63° respectively, ascribed to the presence of NiO. The main diffraction peaks of Ni-RFCC were all maintained with a moderate loss of crystallinity, indicating no major structural changes in the zeolite units after the incorporation of nickel by impregnation method and calcination [38]. However, Ni-ARFCC completely lost its crystallinity as result of the calcination step after doping. Indeed, it has been reported that zeolite Na-A undergoes dehydration and dihydroxylation, and consequent collapsing of its crystal structure upon thermal treatment. This behaviour is in agreement with the major drop in BET surface area moving from ARFCC to Ni-ARFCC (see Textural properties section) [39]. In addition, Ni-RFCC and Ni-ARFCC show diffraction peaks ascribed to nickel aluminate ($NiAl_2O_4$) spinel peaks [35,40].

SEM images in the Fig. 3 reveal the distinct morphologies of various zeolite samples. Fig. 3(a) shows the cubic shapes characteristic of commercial ZSM-5 zeolite, while Fig. 3(b) captures the spherical particles typical of Beta zeolite [41,42]. In Fig. 3(c), the granular structure of FCCC particles, predominantly made up of zeolite Y, is evident [5]. Lastly, image (d) exhibits crystals with the classic octahedral and cubic structures associated with Na-X and Na-A zeolites, respectively, as seen in the ARFCC sample [5]. As well depicted in the XRD characterization, SEM images of the doped supports (Figure S1) show that all the samples retained the same morphologies observed in Fig. 3, except for sample Ni-ARFCC where the typical cubic structure of zeolite Na-A is no longer visible.

The TEM-EDX analysis was conducted on the synthesized catalysts to evaluate the nickel distribution on the zeolite structures, as depicted in Fig. 4. Well defined nickel nanoparticles were not distinctly visible in the EDX maps, indicating that nickel was evenly dispersed across the support structure. Notably, the analysis revealed nanosheets on all the treated supports (Fig. 4 a to d), with no evidence of nickel agglomeration. TEM images were used to calculate the Ni particles size and their distributions by mean of an image processing software (see Table S3 and Figure S4), revealing a log-normal distribution with average particles in the 17 to 25 nm range.

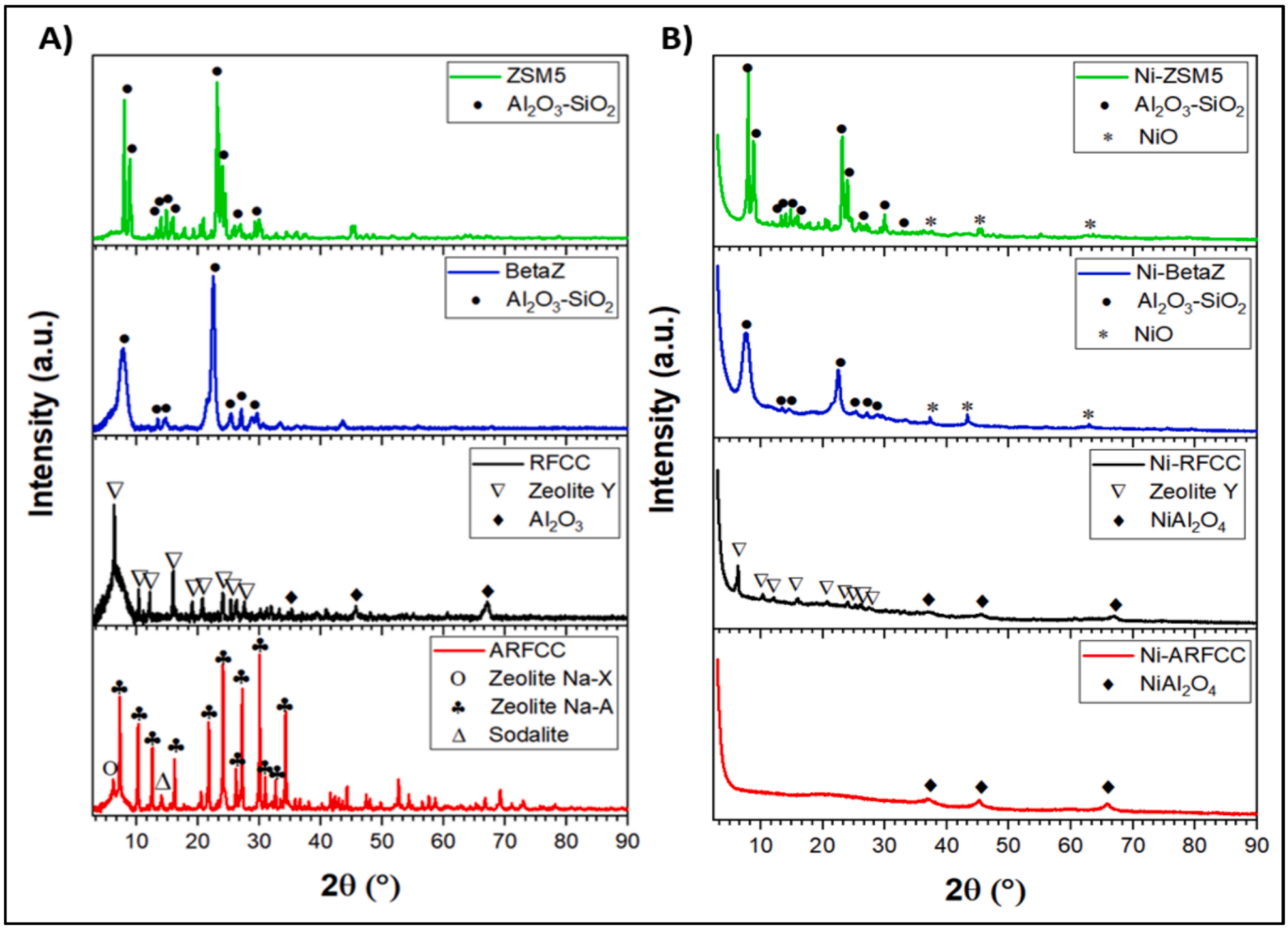

Fig. 2. XRD patterns of pristine zeolites samples (A) and Ni doped-zeolites catalysts (B).

3.2. *Textural properties*

Figure S2 and S3 present the nitrogen adsorption–desorption isotherms and pore size distributions for the catalyst samples, respectively. Each isotherm is of type IV with a hysteresis loop, suggesting the presence of mesopores according to IUPAC classification [43]. The BET surface areas and pore volumes for the nickel-doped catalysts are compiled in Table 1, and those for the undoped catalysts are collected in Table S1. The BET surface area of the doped commercial zeolites is remarkably higher than that for the doped recycled zeolites with 555 and 391 m^2/g (for Ni-Beta, and Ni-ZSM) against 10 and 97 m^2/g (for Ni-ARFCC, and Ni-RFCC) [39]. In general, after the nickel impregnation, the BET surface area of all the metal-containing catalysts was similar to those of the corresponding undoped zeolite samples, except for Ni-ARFCC. The low surface area for Ni-ARFCC is attributed to the dehydration and dihydroxylation induced by the calcination step after doping (typical of zeolite Na-A), thus the collapse of the zeolite structure.

The H_2-TPR experiments aimed to shed light on the reduction behaviour of the produced catalysts, with Fig. 5 presenting the H_2-TPR profiles for both commercial and recycled zeolite samples. The observed peaks at temperatures under 400 ℃ typically represent the reduction of NiO not integrated into the support structure, while those under 600 ℃ may be attributed to interactions of NiO with the support, possibly indicating the presence of surface $NiAl_2O_4$ spinel or NiO weakly interacting with the support. Peaks occurring over 600 ℃ are associated with the reduction of more complexly bonded metal oxide forms, such as crystalline $NiAl_2O_4$ spinel or strongly adhered NiO species [44–46]. Although nickel spinels can readily form through the reaction between Ni and Al_2O_3, it is suggested that $NiAl_2O_4$ spinel is not easily reduced to Ni^0 species, leading to Ni sites that significantly interact with the support, which is a pivotal factor in the maintenance of Ni's catalytic performance during DRM processes [46].

For the Ni-ZSM5 catalyst, the main reduction was performed at 589℃, indicating a good interaction between the active metal and the support. Two minor peaks at 58 and 230 ℃ confirmed the presence of free NiO, as previously observed in the XRD. Similarly, Ni-BetaZ presented a structured profile with three distinctive peaks at 407, 488, and 620 ℃ suggesting a medium interaction between nickel and the zeolite, plus a small peak at 47 ℃ characteristic of the presence of NiO. The recycled zeolite Ni-RFCC exhibited two consecutive reduction peaks at 554 and 612 ℃, whereas Ni-ARFCC showed a similar pattern but shifted at higher temperatures (662 and 773 ℃). The strong interaction between nickel and alumina in the recycled zeolite can be attributed to their lower Si:Al ratio (approximately 1:1), compared to the commercial supports (25:1 for BetaZ and 30:1 for ZSM-5). In Ni-ARFCC, the reduction peaks are shifted to higher temperature because the acid treatment, together with leaching rare elements, typically causes the formation of cavities and defects in similar materials. These are responsible for strengthening the interaction between NiO and the substrate, and lead to an increase of the interfacial area. Indeed, studies have shown that the etching of silica and/or alumina within clay-based materials, such as halloysites, induces defects and cavities. These features can trap Ni particles, resulting in the creation of a robust metal-support interaction

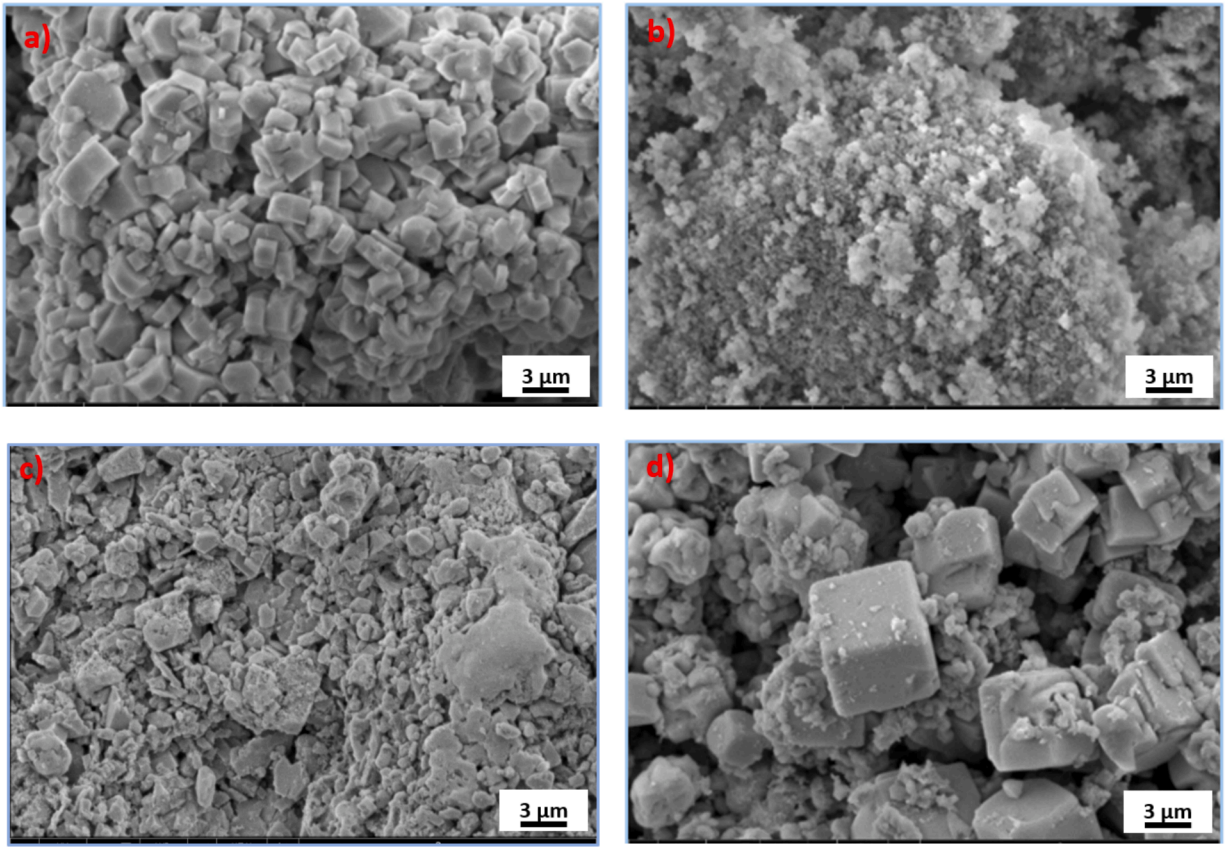

Fig. 3. SEM images of pristine a) ZSM-5, b) BetaZ, c) RFCC, and d) ARFCC.

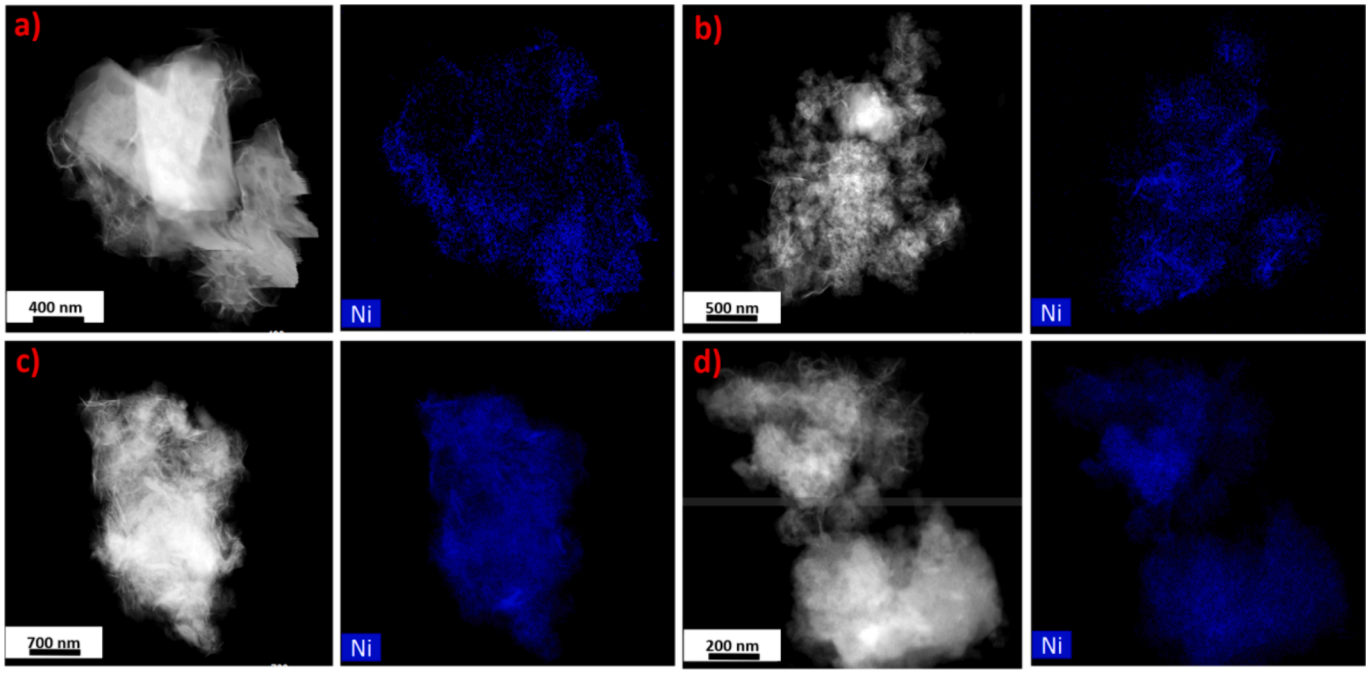

Fig. 4. TEM-EDS analysis images of Ni-doped catalysts a) Ni-ZSM5, b) Ni-BetaZ, c) Ni-RFCC, and d) Ni-ARFCC.

[47–49].

Hydrogen consumption for the catalysts was determined, varying between 29 to 70 cm^3/g at standard temperature and pressure, and it is detailed in Table 2. Catalysts with higher nickel content, particularly commercial supports Ni-ZSM5 and Ni-BetaZ (15.26 and 23.51 Ni wt%, respectively), exhibited greater hydrogen uptake. This can be correlated with their high initial catalytic activity, due to significant Ni loadings identified through H_2-TPR. Notably, Ni-BetaZ recorded the highest H_2 consumption and, accordingly, the highest Ni loading. This can be attributed to the relatively higher surface area, confirming that the order

Table 1
Surface Area & Pore Size Analysis of the doped samples.

Catalyst	BET Surface Area, S_{BET} [m^2/g]	Micropore area [m^2/g]	Total Pore Volume, V_t [cm^3/g]	Average pore size [nm]
Ni-ZSM5	391.21	257.73	0.368	13.45
Ni-BetaZ	555.08	361.58	1.021	18.62
Ni-RFCC	97.12	56.71	0.317	12.83
Ni-ARFCC	9.71	5.41	0.317	33.12

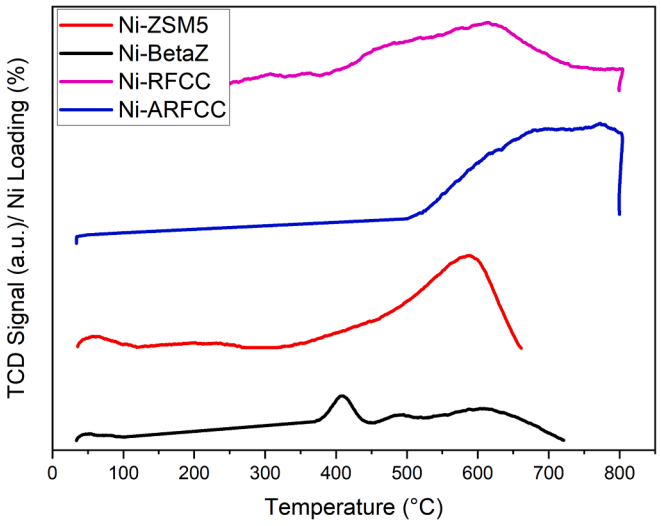

Fig. 5. H_2-TPR Profile of the zeolite-supported Ni catalysts.

of Ni loading follows the same order of surface area: Ni-BetaZ, followed by Ni-ZSM5, Ni-RFCC, and finally Ni-ARFCC.

Nickel dispersion, determined by H_2-Pulse Chemisorption and listed in Table 2, ranges from 0.03 % to 0.47 %, with extremely low values for the recycled samples Ni-RFCC and Ni-ARFCC due to the presence of impurities and the relatively low surface area. This pattern aligns with findings in similar studies on clay-based and mesoporous catalysts. For example, our group obtained comparable values between 0.2 and 2.7 for chemically treated halloysite-based catalyst [49], similarly Zhao *et al.* reported values between 0.17 and 0.6 for modified HNTs [50]. Moreover, these findings from pulse chemisorption experiments indicate that the catalytic reaction may not be solely influenced by the Ni dispersion but it is expression of the combination between multiple physical and chemical parameters specific to the substrate, the catalyst, and the reagents/products.

Nickel loading quantification, discussed earlier with an expected 15 wt% target, showed discrepancies in H_2-TPR outcomes due to the varied adsorption behaviour of Ni^{2+} ions on different zeolite supports. This is indeed influenced by surface characteristics such as presence of terminal groups, cavities, and other cations, as well as differences in surface area, porosity, and water dispersion contributing to the distinct ways in which nickel ions are adsorbed on different zeolite supports.

Ni-ZSM5 and Ni-BetaZ showed one major NH_3 desorption peak, at 136 and 119 °C respectively, which is corresponding to typical weak acid sites [51] followed by featureless desorption band of low intensity between 400–600 ℃. Unlike the commercial supports, both recycled substrates Ni-RFCC and Ni-ARFCC exhibited an uncommon NH_3 desorption profile, with intensity growing up to 350 ℃ and then reaching a plateau (see Fig. 6). The composition of these two samples is quite complex, together with Al and Si they include small percentages of V, Ti, Fe, La, etc. (see XRF analysis in Table 3), therefore we assume that the presence of such impurities might affect the desorption profile of the samples.

3.3. Catalyst activity & stability evaluation

Given that dry reforming of methane (DRM) is an endothermic reaction, it requires high temperatures, typically between 627–1000 ℃, and atmospheric pressure to achieve equilibrium conversion, limit carbon buildup, and maintain stability [52]. The catalysts' performances were tested at 750 ℃, where the conversion rates of CH_4 and CO_2, and the H_2/CO ratio were determined. From Fig. 7, it can be noted that CO_2 conversion exceeded that of CH_4 across all catalysts, with Ni-ARFCC exhibiting the highest conversions of both gases and maintaining exceptional stability with minimal coke formation over a continuous 20-hour period. On the other hand, Ni-RFCC depicted the lowest overall CH_4 conversion (11.67 %) and the lowest CO_2 conversion (15 %). In terms of H_2/CO ratio, Ni-ZSM5, Ni-BetaZ, and Ni-ARFCC resulted in a final average value of 0.75 (Fig. 7), as effect of the reverse water–gas

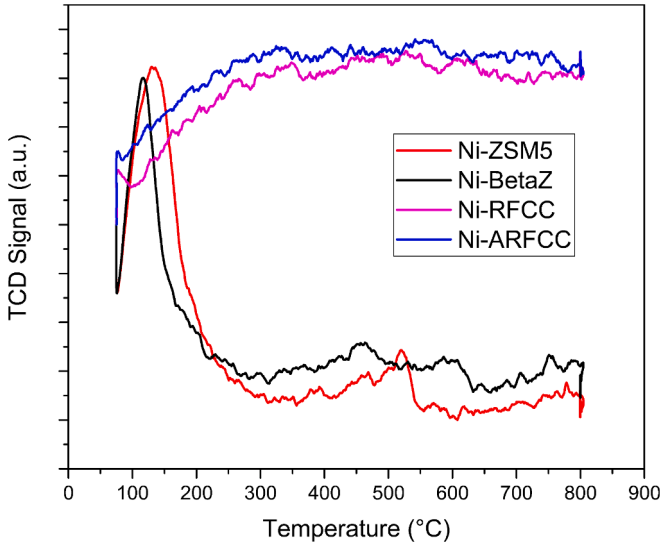

Fig. 6. NH_3-TPD profile of the zeolite-supported Ni catalysts.

Table 2
H_2-TPR, NH_3-TPD and H_2-Pulsechemisorption analysis.

Catalyst	H_2-TPR			H_2-Pulse Chemisorption	NH_3-TPD	SEM/EDS
	Peaks (°C)	**Quantity (cm^3/g STP)**	**Ni Loading (%)**	**Ni Dispersion (%)**	**Peaks (°C)**	**Si/Al**
Ni-ZSM5	58, 230, 589	45.77	15.26	0.47	136	34.70
Ni-BetaZ	47, 407, 488, 620	70.55	23.51	0.31	119	16.94
Ni-RFCC	554, 612	36.07	12.02	0.03	75	0.97
Ni-ARFCC	662, 773	29.41	9.80	0.06	78	1.24

Table 3
XRF analysis of undoped recycled zeolites RFCC and ARFCC [5].

		Concentration (wt%)								
Sample	Na	Al	Si	P	Ti	V	Fe	Ni	La	Ce
RFCC	–	15.60	12.30	0.13	0.47	0.050	0.25	0.03	2.30	0.16
ARFCC	7.98	11.59	11.74	–	0.45	0.005	0.19	0.03	0.33	0.03

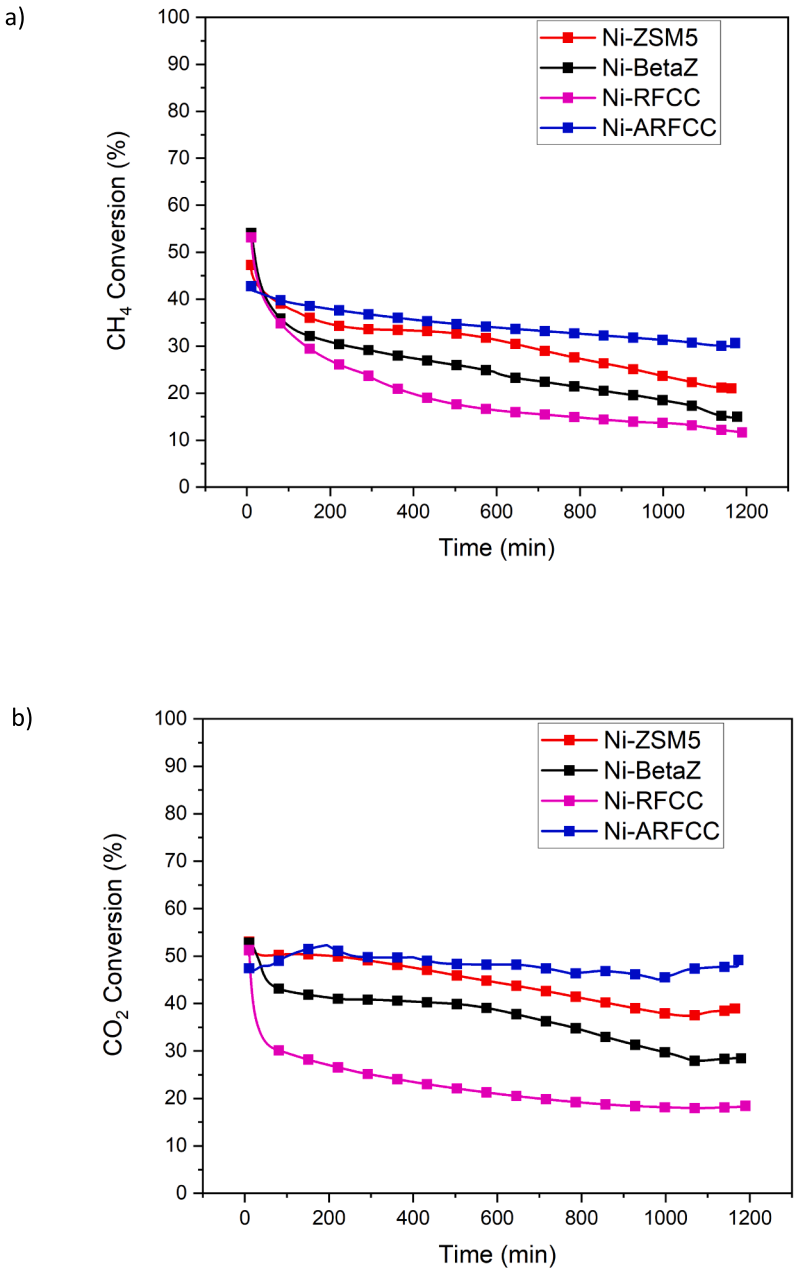

Fig. 7. Catalytic performances of the studied catalysts a) CH_4 conversion b) CO_2 conversion c) H_2/CO molar ratio.

shift reaction. In contrast, the Ni-RFCC showed a different performance, experiencing a significant drop in CO_2 conversion with over a 30 % decrease. Additionally, it exhibited a relatively higher H_2/CO ratio. These two phenomena occurred due to the water gas shift reaction $CO + H_2O \rightleftharpoons CO_2 + H_2$, which favours the presence of La and Ce, elements that exist in this catalyst (see Table 3) [53].

Fig. 7 indicates that the Ni-ARFCC catalyst demonstrated a consistent performance, showing no significant loss in the conversion of CH_4 and

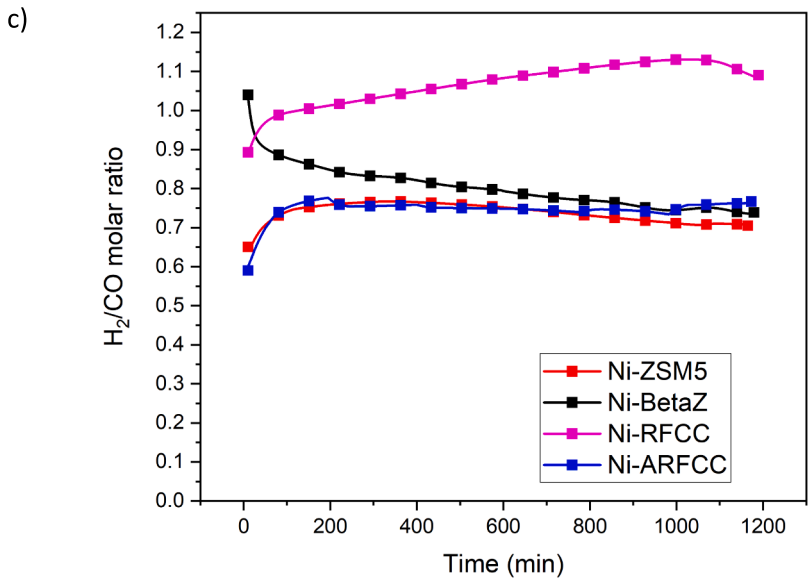

Fig. 7. (*continued*).

CO_2 over a testing period of 20 h, which suggests stable catalytic activity. Such behaviour and stability can be explained thanks to the presence of sodium in the catalyst (~8 wt%, see Table 3). In fact, previous studies have demonstrated that the interaction with sodium has a beneficial effect on supported catalysts, reducing the accumulation of carbon on the spent catalyst's surface. This suggests that sodium could potentially extend the catalyst's lifespan by avoiding coke deposition, a factor that might otherwise result in catalyst poisoning [19]. Given that sodium oxide is a potent base, the presence of sodium indicates the existence of in situ basic sites on the Ni-ARFCC (derived from zeolite Na-A), ensuring effective CO_2 activation. Whereas for Ni-RFCC, a significant deactivation was observed, with the conversion dropping from 53 % to 12 % (CH_4) and 51 % to 18 % (CO_2), after 20 hrs.

The greater initial methane conversion observed in the commercial zeolite-supported catalysts and Ni-RFCC is linked to their higher H_2 consumption, as shown by H_2-TPR results, and their increased nickel content. While all the samples showed similar initial CO_2 adsorption levels, the Ni-ARFCC sample displayed a minimal decrease in CO_2 conversion, corresponding to −1.6 %, according to the data in Table 4.

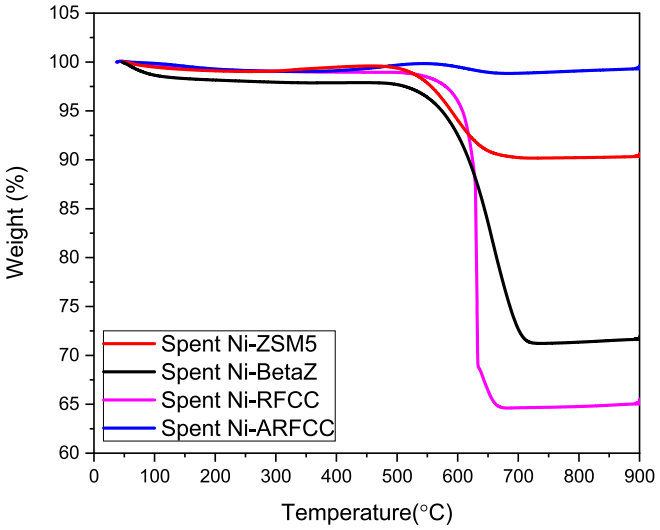

Fig. 8. TGA analysis of the spent catalysts.

3.4. Spent catalyst characterization

Following the 20-hour dry reforming of methane experiments, the catalysts were cooled to ambient temperature, and then analysed using TGA, TEM, and XPS to assess coke deposition (comparison of XPS spectra of fresh and spent catalyst is depicted in Figures S8-S11). The results are presented in Fig. 8, Fig. 9, and Fig. 10, respectively. Additionally, Table 4 lists the percentages of coke deposited on the catalysts in terms of weight %, as determined by TGA, after the reactions at 750 °C. For all samples, excluding Ni-ARFCC, a significant weight % loss was observed in the TGA profiles, occurring at temperatures ranging from 450 to 550 °C and at 550–650 °C for Ni-RFCC. For Ni-RFCC, this suggests the presence of a predominant morphology of deposited carbon coke on the catalyst. Generally, the temperature of weight losses in the TGA profile provides insights into the carbon type, while the intensity of these signals indicates the quantity of formed coke. The temperature range where the main loss was observed for the spent commercial zeolites is associated with the temperature at which both amorphous carbon and filamentous carbon forms coexist. In fact, the C1s XPS spectra for

Table 4
Catalyst Performance Parameters.

Catalyst	CH_4 Conversion[%]		CO_2 Conversion[%]		Coke formation [%]	Average Ni particle size increase due to sintering [nm]
	t = 10 [min]	**t = 1200 [min]**	**t = 10 [min]**	**t = 1200 [min]**		
Ni-ZSM5	47.31	21.04	53.07	38.84	9.8	+3.78
Ni-BetaZ	54.14	14.99	52.80	28.58	28.5	+6.56
Ni-RFCC	53.17	11.67	51.28	18.45	35.3	+8.55
Ni-ARFCC	42.78	30.78	47.46	49.18	1.2	+31.77

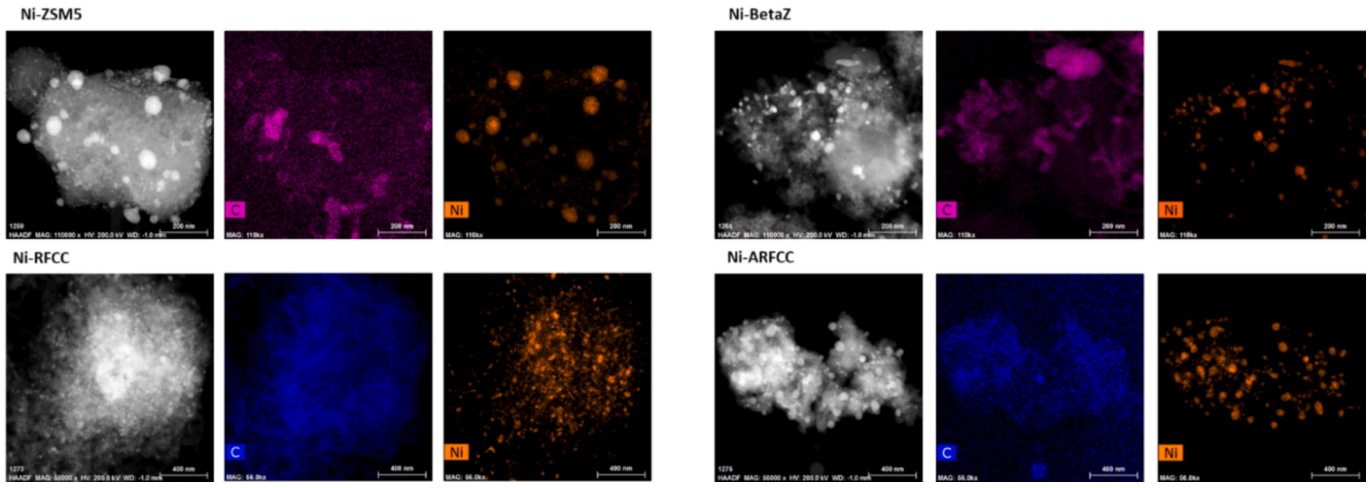

Fig. 9. TEM images and EDX Nickel and Carbon elemental mapping of the spent catalysts.

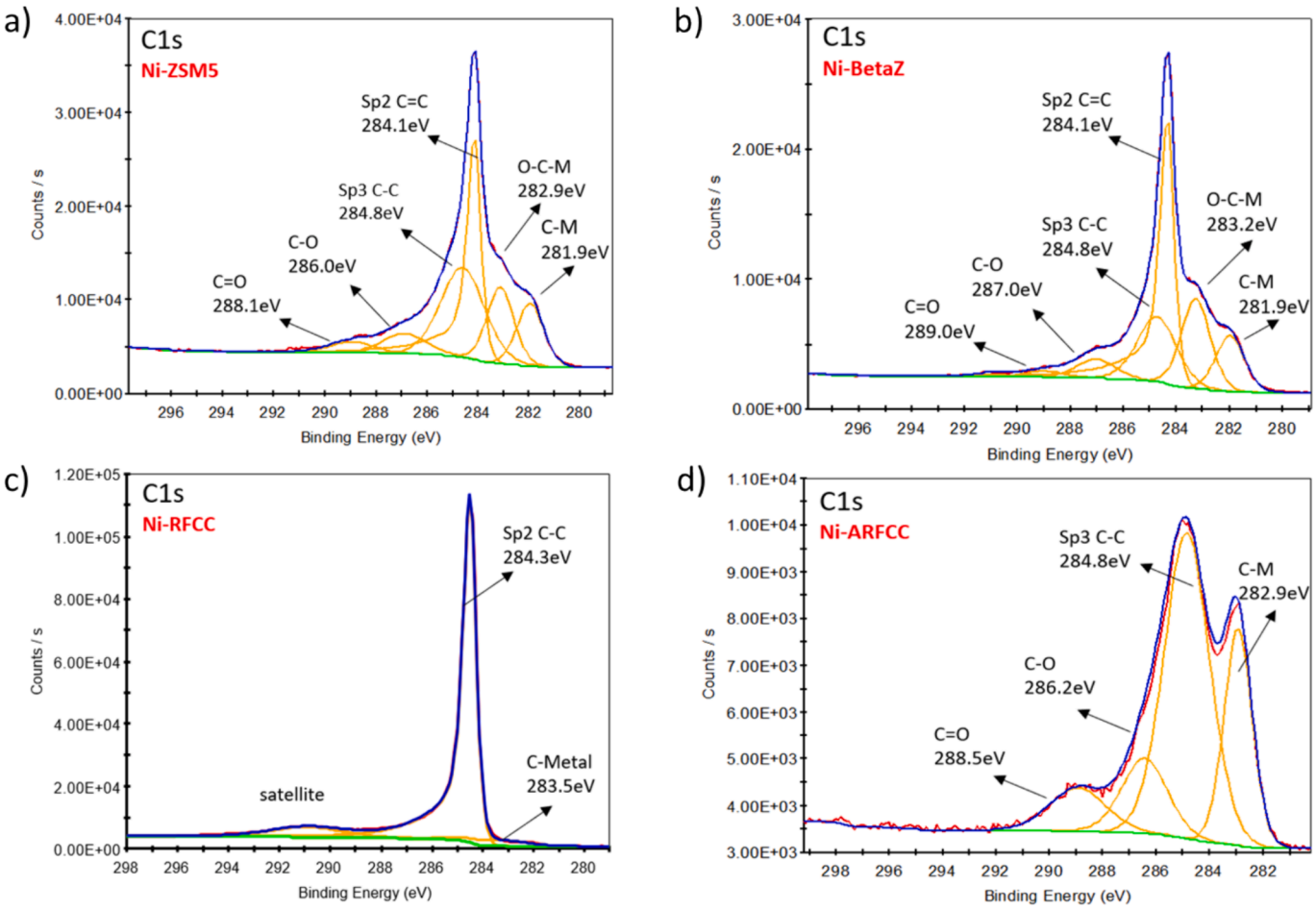

Fig. 10. XPS analysis and deconvolution of C1s peaks of a) Ni-ZSM5, b) Ni-BetaZ, c) Ni-RFCC and d) Ni-ARFCC.

these two catalysts are quite similar indicating the presence of both sp2 and sp3 carbon, typical of graphitic and amorphous carbon, respectively. TEM images in Fig. 11 have confirmed the two morphologies. Whereas the higher temperature indicated for the weight loss in Ni-RFCC is more in favour of carbon filaments only, as confirmed in the corresponding C1s XPS spectrum (Fig. 10), which presents exclusively sp2 carbon, and TEM image (Fig. 11), which shows a tangle of carbon filaments. Ni-ARFCC had a different behaviour compared to the other catalysts. We did not record significant weight losses, instead a minimal weight gain was observed around 543 ℃, attributed to nickel oxidation. Small amount of carbon, deposited around the nickel have been observed by TEM and confirmed by the XPS analysis.

The XPS analysis of the spent catalyst also revealed some interesting features for Ni2p, Si2p, and Al2p signals when comparing fresh with spent catalysts (Figures S8-S11). In particular, in the Ni2p profile for spent samples Ni-RFCC and Ni-BetaZ, we observed an extremely weak

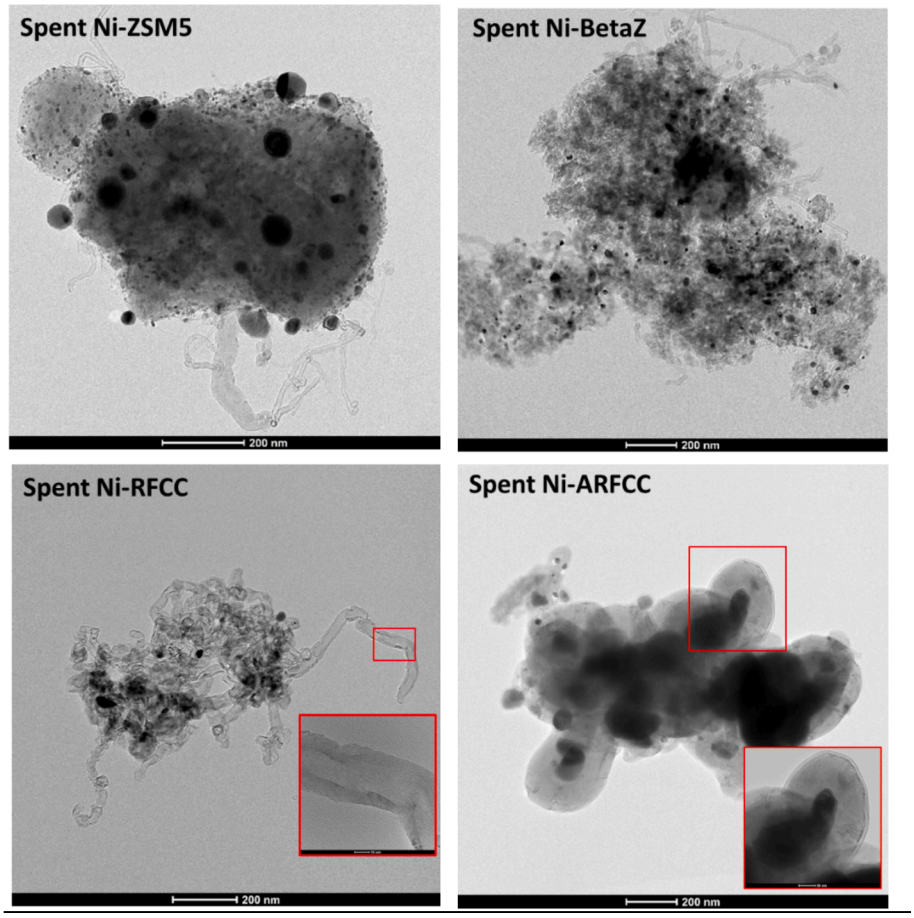

Fig. 11. TEM images reporting the detail of the carbon deposition on the spent commercial catalysts (top) and on detached Ni nanoparticles for the spent samples Ni-RFCC and Ni-ARFCC (bottom).

featureless signal, in agreement with the high coke deposition observed for the two catalysts (Fig. 8), able to coat the nickel particles and shield their XPS response. For spent samples Ni-ARFCC and Ni-ZSM5, Ni2p spectrum is weaker than that for the corresponding fresh catalysts but still visible, with the appearance of a peak at 851.3 eV attributed to the formation of Ni-C bond. Despite low or no nickel has been detected by XPS, nickel is still present in all the spent catalysts as depicted in Fig. 9 and Figure S12. When looking at the Si2p spectra of the spent catalysts, we generally observed a shift of the main peak to lower energy, when compared to the spectra of the corresponding fresh catalysts. This shift is attributed to the formation of C-Si-O and Si-O-C bonds, again due to the coke deposition. In fact, the shift in Si2p spectrum for spent Ni-ARFCC was only minimal, in agreement its high catalytic stability and low carbon formation. It is important to note that the silicon XPS spectra for all the spent catalysts could have been affected by the presence of glass wool, a silicon-based material used for packing the catalyst inside the reactor. The presence of glass wool fibres has been observed in the SEM images of the spent catalysts, with typical tubular silicon oxide formations (Figure S12). The profile of Al2p spectra of the spent catalysts have been mainly affected by the drastic reduction in the Ni3p signals at 69.3 and 71 eV, which generally overlap with the Al2p peaks of the fresh catalysts. As discussed for the Ni2p signals, the intensity drop for Ni3p peaks is attributed to the deposition of coke on the nickel particles.

The weight loss percentages depicted in Fig. 9 well align with the catalysts' performance in terms of CH_4 and CO_2 conversion stability. Specifically, Ni-ARFCC demonstrates minimal deactivation over 20 h, correlating with the lowest coke formation, as confirmed by the minimal weight loss in its TGA profile. The TGA analysis reveals that catalysts using commercial substrates undergo more coke formation than those using recycled supports. It is worth mentioning that the TGA profiles of the undoped and fresh catalysts are reflected in Figure S6 and Figure S7, respectively. For those, it was noted that only one drop around 100 °C is shown, indicating the moisture content.

TEM analysis in Fig. 8 confirmed the sintering effect on nickel within the spent catalysts, highlighting the growth of nickel nanoparticles to sizes as large as 130 nm. Analysis of particle size distribution, detailed in Table S2, and Figure S5, indicated that the average size of nanoparticles in spent catalysts was between 20 to 30 nm.

In Fig. 11 are reported TEM images that better depict the presence of both amorphous carbon and carbon filaments in the spent catalysts. These materials progressively build up on the support surface through the transformation of active surface carbons over the course of the reaction time, ultimately resulting in catalyst deactivation. Differently from the commercial zeolites-based catalysts, for the spent Ni-RFCC and Ni-ARFCC samples we observed detaching and lifting of Ni nanoparticles from the catalyst surface, with potentially a combination of tip-growth/base growth mechanisms.

In Ni-RFCC we observed carbon accumulation in the form of MWCNTs (Fig. 11). Similar behaviour has been reported for DRM catalysts containing La_2O_3 (pristine RFCC contains 2.3 wt% of La) [21,54]. Whereas in Ni-ARFCC, where most of the lanthanum has been chemically leached, we still observed Ni nanoparticle detachment with shell-like deposition of carbon, also confirmed by the presence of carbon sp3 peak in the XPS spectrum.

4. Conclusion

This study focused on the utilization of zeolite-based materials,

particularly those obtained from spent fluid catalyst cracking (FCC) processes, as catalyst supports for Ni-based catalysts in the dry reforming of methane (DRM) reaction. Zeolites were chosen for their well-defined pore structure, abundance, chemical/thermal stability, and high surface area. TEM-EDX analysis showed well-distributed nickel nanoparticles on the supports, and no significant agglomeration. The BET surface area of the doped commercial zeolites was significantly higher than that of the recycled zeolites, especially Ni-ARFCC, which experienced a notable decrease in surface area due to dehydration and dihydroxylation during the calcination step. H_2-TPR experiments were conducted to investigate the reduction behaviour of the catalysts, revealing different reduction profiles for the commercial and recycled zeolite-supported Ni catalysts. The recycled zeolite-supported catalysts exhibited higher reduction peaks at elevated temperatures, indicating a strong interaction between nickel and alumina, attributed to the lower Si:Al ratio in the recycled supports.

Catalyst activity and stability evaluation at 750 ℃ in the DRM reaction showed varying performance among the catalysts. Ni-ARFCC demonstrated the highest overall CO_2 and CH_4 conversions, with remarkable stability and negligible coke deposition over 20 h. In contrast, Ni-RFCC exhibited the lowest overall conversions and higher coke formation. The presence of sodium in Ni-ARFCC was suggested to contribute to its stability by minimizing carbon deposition. TGA and TEM analyses of spent catalysts confirmed the presence of mainly filamentous carbon, with Ni-ARFCC showing the least coke formation and stable performance. TEM analysis also revealed a modest sintering effect on nickel nanoparticles in all spent catalysts.

In summary, the study highlights the potential of reusing zeolite-based materials from spent FCCs as catalyst supports for Ni-based catalysts in DRM. The choice of zeolite type, surface area, and interactions between nickel and support materials significantly influenced the catalyst's structural, textural, and catalytic properties, providing insights for further optimization in the development of efficient DRM catalysts.

CRediT authorship contribution statement

Ahmed Abotaleb: Writing – review & editing, Writing – original draft, Investigation, Formal analysis, Conceptualization. **Nada Abounahia:** Writing – original draft, Investigation. **Sjood Makeen:** Investigation. **Janarthanan Ponraj:** Formal analysis. **Mabkhout Al Yarabah:** Investigation. **Francesco Ferella:** Writing – review & editing, Writing – original draft. **Alessandro Sinopoli:** Writing – review & editing, Writing – original draft, Validation, Supervision, Investigation, Conceptualization.

Declaration of competing interest

The authors declare that they have no known competing financial interests or personal relationships that could have appeared to influence the work reported in this paper.

Data availability

No data was used for the research described in the article.

Acknowledgements

The authors acknowledge Qatar Environment and Energy Research Institute (QEERI, at Hamad Bin Khalifa University) for supporting this research. The authors would like also to thank the core lab staff at Hamad Bin Khalifa University, namely Dr. Akshath Raghu Shetty, Dr. Yongfeng Tong, Abdulaziz M. Al-Emadi, Dr. Atef Zekri, and Omar Al Hassan for their material characterization support.

Appendix A. Supplementary material

Supplementary data to this article can be found online at https://doi.org/10.1016/j.fuel.2024.132356.

References

[1] Harrington LMB. Sustainability theory and conceptual considerations: a review of key ideas for sustainability, and the rural context. Pap Appl Geogr 2016;2:365–82. https://doi.org/10.1080/23754931.2016.1239222.
[2] Nations U. The 2030 Agenda and the Sustainable Development Goals; 2023.
[3] Ferella F, De Michelis I, Beolchini F, Innocenzi V, Vegliò F. Extraction of zinc and manganese from alkaline and zinc-carbon spent batteries by citric-sulphuric acid solution. Int J Chem Eng 2010;1–13:2010. https://doi.org/10.1155/2010/659434.
[4] Alonso-Fariñas B, Rodríguez-Galán M, Arenas C, Arroyo Torralvo F, Leiva C. Sustainable management of spent fluid catalytic cracking catalyst from a circular economy approach. Waste Manag 2020;110:10–9. https://doi.org/10.1016/j.wasman.2020.04.046.
[5] Ferella F, et al. Synthesis of zeolites from spent fluid catalytic cracking catalyst. J Clean Prod 2019;230:910–26. https://doi.org/10.1016/j.jclepro.2019.05.175.
[6] Ferella F, Innocenzi V, Maggiore F. Oil refining spent catalysts: A review of possible recycling technologies. Resour Conserv Recycl 2016;108:10–20. https://doi.org/10.1016/j.resconrec.2016.01.010.
[7] Bapco, B. P. C. <https://www.bapco.net/en/page/introduction/> (2024).
[8] Commission, E. *Critical raw materials*, <https://single-market-economy.ec.europa.eu/sectors/raw-materials/areas-specific-interest/critical-raw-materials_en>.
[9] Innocenzi V, Ferella F, De Michelis I, Vegliò F. Treatment of fluid catalytic cracking spent catalysts to recover lanthanum and cerium: comparison between selective precipitation and solvent extraction. J Ind Eng Chem 2015;24:92–7. https://doi.org/10.1016/j.jiec.2014.09.014.
[10] Innocenzi V, Ferella F, Innocenzi V, De Michelis I, Vegliò F. Process for the recovery of rare earth elements. Italy patentl; 2012.
[11] Hambali HU, et al. Zeolite and clay based catalysts for CO2 reforming of methane to syngas: a review. Int J Hydrogen Energy 2022;47:30759–87. https://doi.org/10.1016/j.ijhydene.2021.12.214.
[12] Ferella F, et al. Spent FCC E-cat: towards a circular approach in the oil refining industry. Sustainability 2019;11:113.
[13] Basaldella EI, Paladino JC, Solari M, Valle GM. Exhausted fluid catalytic cracking catalysts as raw materials for zeolite synthesis. Appl Catal B 2006;66:186–91. https://doi.org/10.1016/j.apcatb.2006.03.013.
[14] Bacariza C, Karam L, El Hassan N, Lopes JM, Henriques C. Carbon dioxide reforming of methane over nickel-supported zeolites: a screening study. Processes 2022;10:1331.
[15] Arora S, Prasad R. An overview on dry reforming of methane: strategies to reduce carbonaceous deactivation of catalysts. RSC Adv 2016;6:108668–88. https://doi.org/10.1039/c6ra20450c.
[16] Bacariza C, Karam L, El Hassan N, Lopes JM, Henriques C. Carbon dioxide reforming of methane over nickel-supported zeolites: a screening study. Processes 2022;10. https://doi.org/10.3390/pr10071331.
[17] Pham Minh D. et al. in Hydrogen Supply Chains 2018;111-166.
[18] Rostrup-Nielsen JR, Sehested J, Noerskov JK. Hydrogen and synthesis gas by steam- and CO2 reforming. ChemInform 2003;34. https://doi.org/10.1002/chin.200317288.
[19] Shittu TD, Ayodele OB. Experimental and computational investigation of CO2–CH4 reforming to syngas over zeolite A supported oxalate ligands functionalized Ni catalysts. Result Eng 2022;16. https://doi.org/10.1016/j.rineng.2022.100630.
[20] Kweon S, Oh S, Lee S, Min H-K, Park MB. Nickel nanoparticles supported on magnesium silicate MWW molecular sieve as an efficient catalyst for dry reforming of methane. Chem Eng J 2023;476:146598. https://doi.org/10.1016/j.cej.2023.146598.
[21] Muñoz HJ, Korili SA, Gil A. Facile synthesis of an Ni/LaAlO3 – perovskite via an MOF gel precursor for the dry reforming of methane. Catal Today 2023;114487. https://doi.org/10.1016/j.cattod.2023.114487.
[22] Cheng Q, et al. Highly efficient and stable methane dry reforming enabled by a single-site cationic Ni catalyst. J Am Chem Soc 2023;145:25109–19. https://doi.org/10.1021/jacs.3c04581.
[23] Fakeeha AH, Khan WU, Al-Fatesh AS, Abasaeed AE. Stabilities of zeolite-supported Ni catalysts for dry reforming of methane. Chin J Catal 2013;34:764–8. https://doi.org/10.1016/s1872-2067(12)60554-3.
[24] Pinheiro AN, Valentini A, Sasaki JM, Oliveira AC. Highly stable dealuminated zeolite support for the production of hydrogen by dry reforming of methane. Appl Catal A 2009;355:156–68. https://doi.org/10.1016/j.apcata.2008.12.007.
[25] Frontera P, et al. Catalytic dry-reforming on Ni–zeolite supported catalyst. Catal Today 2012;179:52–60. https://doi.org/10.1016/j.cattod.2011.07.039.
[26] Wei Q, et al. Ni/Silicalite-1 coating being coated on SiC foam: A tailor-made monolith catalyst for syngas production using a combined methane reforming process. Chem Eng J 2017;327:465–73. https://doi.org/10.1016/j.cej.2017.06.109.
[27] Kweon S, et al. Defect-stabilized nickel on beta zeolite as a promising catalyst for dry reforming of methane. Cat Sci Technol 2022;12:3106–15.
[28] Najfach AJ, Almquist CB, Edelmann RE. Effect of Manganese and zeolite composition on zeolite-supported Ni-catalysts for dry reforming of methane. Catal Today 2021;369:31–47. https://doi.org/10.1016/j.cattod.2020.07.058.

[29] Liang D, et al. Dry reforming of methane for syngas production over attapulgite-derived MFI zeolite encapsulated bimetallic Ni-Co catalysts. Appl Catal B 2023; 322. https://doi.org/10.1016/j.apcatb.2022.122088.
[30] Zhu Q, et al. Zeolite fixed cobalt–nickel nanoparticles for coking and sintering resistance in dry reforming of methane. Chem Eng Sci 2023;280. https://doi.org/10.1016/j.ces.2023.119030.
[31] Miao C, Chen S, Shang K, Liang L, Ouyang J. Highly active Ni–Ru bimetallic catalyst integrated with MFI zeolite-loaded cerium zirconium oxide for dry reforming of methane. ACS Appl Mater Interfaces 2022;14:47616–32.
[32] Auer E, Freund A, Pietsch J, Tacke T. Carbons as supports for industrial precious metal catalysts. Appl Catal A 1998;173:259–71.
[33] Quindimil A, De-La-Torre U, Pereda-Ayo B, González-Marcos JA, González-Velasco JR. Ni catalysts with La as promoter supported over Y- and BETA- zeolites for CO2 methanation. Appl Catal B 2018;238:393–403. https://doi.org/10.1016/j.apcatb.2018.07.034.
[34] Wei L, et al. Influence of nickel precursors on the properties and performance of Ni impregnated zeolite 5A and 13X catalysts in CO2 methanation. Catal Today 2021; 362:35–46. https://doi.org/10.1016/j.cattod.2020.05.025.
[35] Bacariza MC, Maleval M, Graça I, Lopes JM, Henriques C. Power-to-methane over Ni/zeolites: Influence of the framework type. Microporous Mesoporous Mater 2019;274:102–12. https://doi.org/10.1016/j.micromeso.2018.07.037.
[36] Wang F, et al. CO 2 reforming with methane over small-sized Ni@SiO 2 catalysts with unique features of sintering-free and low carbon. Appl Catal B 2018;235: 26–35. https://doi.org/10.1016/j.apcatb.2018.04.069.
[37] Xu J, Zhang T. Fabrication of spent FCC catalyst composites by loaded V(2)O(5) and TiO(2) and their comparative photocatalytic activities. Sci Rep 2019;9:11099. https://doi.org/10.1038/s41598-019-47155-y.
[38] Wei Q, et al. Synthesis of Ni-modified ZSM-5 zeolites and their catalytic performance in n-octane hydroconversion. Front Chem 2020;8:586445. https://doi.org/10.3389/fchem.2020.586445.
[39] Krol MK, Jelen P. The effect of heat treatment on the structure of zeolite A. Materials (Basel) 2021;14. https://doi.org/10.3390/ma14164642.
[40] Graça I, et al. CO2 hydrogenation into CH4 on NiHNaUSY zeolites. Appl Catal B 2014;147:101–10. https://doi.org/10.1016/j.apcatb.2013.08.010.
[41] Tehubijuluw H, Subagyo R, Kusumawati Y, Prasetyoko D. The impregnation of ZnO onto ZSM-5 derived from red mud for photocatalytic degradation of methylene blue. Sustain Environ Res 2022;32. https://doi.org/10.1186/s42834-021-00113-8.
[42] Kweon S, Kim YW, Shin C-H, Park MB, Min H-K. Nickel silicate beta zeolite prepared by interzeolite transformation: a highly active and stable catalyst for dry reforming of methane. Chem Eng J 2022;431. https://doi.org/10.1016/j.cej.2021.133364.
[43] Lin T, et al. Halloysite nanotube functionalized with La-Ca bimetallic oxides as novel transesterification catalyst for biodiesel production with molecular simulation. Energ Conver Manage 2020;220:113138.
[44] Zhao Z, Ren P, Li W. Supported Ni catalyst on a natural halloysite derived silica–alumina composite oxide with unexpected coke-resistant stability for steam-CO 2 dual reforming of methane. RSC Adv 2016;6:49487–96.
[45] Wu T, Li S, Yan Q. Effect of interaction between nickel and alumina on coke deposition on Ni/Al~ 2O–3 catalyst for partial oxidation of methane to syngas. Chin J Catal 2001;22:504–6.
[46] Zhou L, Li L, Wei N, Li J, Basset JM. Effect of NiAl2O4 formation on Ni/Al2O3 stability during dry reforming of methane. ChemCatChem 2015;7:2508–16.
[47] Bakhtiari K, Kootenaei AS, Maghsoodi S, Azizi S, Ghomsheh SMT. Synthesis of high sintering-resistant Ni-modified halloysite based catalysts containing La, Ce, and Co for dry reforming of methane. Ceram Int 2022;48:37394–402.
[48] Lu M, et al. Coke-resistant defect-confined Ni-based nanosheet-like catalysts derived from halloysites for CO 2 reforming of methane. Nanoscale 2018;10: 10528–37.
[49] Abotaleb A, et al. Assessing the effect of acid and alkali treatment on a halloysite-based catalyst for dry reforming of methane. RSC Adv 2024;14:4788–803. https://doi.org/10.1039/D3RA07990B.
[50] Zhao Z, Ren P, Li W. Supported Ni catalyst on a natural halloysite derived silica–alumina composite oxide with unexpected coke-resistant stability for steam-CO2 dual reforming of methane. RSC Adv 2016;6:49487–96. https://doi.org/10.1039/c6ra09203a.
[51] Kweon S, An H, Shin C-H, Park MB, Min H-K. Nitrided Ni/N-zeolites as efficient catalysts for the dry reforming of methane. J CO2 Util 2021;46:101478. https://doi.org/10.1016/j.jcou.2021.101478.
[52] Sharifianjazi F. et al. A review on recent advances in dry reforming of methane over Ni-and Co-based nanocatalysts. Int J Hydrogen Energy 2022;47:42213-42233.
[53] Wang Y, Liang S, Cao A, Thompson RL, Veser G. Au-mixed lanthanum/cerium oxide catalysts for water gas shift. Appl Catal B 2010;99:89–95. https://doi.org/10.1016/j.apcatb.2010.06.004.
[54] Zhao H, et al. Highly coke-resistant Ni-La2O2CO3 catalyst with low Ni loading for dry reforming of methane with carbon dioxide. Catal Today 2022;402:189–201. https://doi.org/10.1016/j.cattod.2022.03.038.